JGR Earth Surface

RESEARCH ARTICLE
10.1029/2019JF005341

Seepage Erosion in the Luquillo Mountains, Puerto Rico, Relict Landscapes

E. J. Harrison[1], G. Y. Brocard[2], N. M. Gasparini[3], N. J. Lyons[3], and J. K. Willenbring[1]

[1]Scripps Institution of Oceanography, University of California San Diego, La Jolla, CA, USA, [2]Institut des Sciences de la Terre, Observatoire des Sciences de l'Univers, University of Grenoble, Grenoble, France, [3]Department of Earth and Environmental Sciences, Tulane University, New Orleans, LA, USA

Key Points:
- Morphology of channels mimics theoretical expectations of groundwater-driven erosion
- Baseflow discharge from springs can transport the fluvial bedload
- Long-term erosion rates scale linearly with baseflow discharge rates

Correspondence to:
E. J. Harrison,
ejharris@ucsd.edu

Citation:
Harrison, E. J., Brocard, G. Y., Gasparini, N. M., Lyons, N. J., & Willenbring, J. K. (2020). Seepage erosion in the Luquillo Mountains, Puerto Rico, relict landscapes. *Journal of Geophysical Research: Earth Surface*, *125*, e2019JF005341. https://doi.org/10.1029/2019JF005341

Received 27 AUG 2019
Accepted 3 APR 2020
Accepted article online 16 APR 2020

Abstract Seminal research into geomorphic shaping of landscapes by emerging groundwater suggest that the relationships governing channel form and incision rate are distinct from other fluvial systems (Howard, 1995; Dunne, 1980, 1990). While some recent work has connected these models to natural settings (Abrams et al., 2009; Petroff et al., 2011), other studies have shown that seepage erosion may be erroneously invoked in landscapes shaped by flooding and overland flow (Lamb et al., 2006, 2007). We investigate the impact of seepage erosion on the geomorphology of a tropical mountain watershed, the Rio Blanco in the Luquillo Mountains of northern Puerto Rico. We focus on a population of amphitheater-shaped channels that incise into deeply weathered saprolite profiles in the upland reaches of the watershed, where the river is disconnected from regional base-level lowering (Brocard et al., 2015, 2016). We measured high rates of baseflow from springs feeding these catchments, despite their small drainage areas. We constructed an empirical model relating baseflow discharge to catchment area within the watershed. We quantified long-term (103-104 yrs) catchment erosion from 10Be in sediment and measured the short-term volumetric flux of bedload transport at baseflow. Rates of transport and erosion in this group of channels scale linearly with the feeding drainage area and baseflow discharge. This finding supports a stream incision model proposed for groundwater-driven channels (Howard, 1995). We propose that deepening saprolite and coincident entrenchment of the subsurface water-routing system initiated seepage erosion and are actively expanding the headwaters in the Rio Blanco.

Plain Language Summary The relationship between landforms and the processes that shape them on Earth can be used to identify the processes at work in places that can only be studied remotely, like the deep ocean or the surface of other planets. In the early 1980s, researchers recognized that river channels have different shapes depending on whether they are carved by water moving over the land surface or flowing underground. Early studies of groundwater erosion in sandbox models found that there is a unique relationship between erosion and the rate of groundwater flow into a channel that does not exist under other circumstances. However, this relationship has yet to be verified in natural landscapes. In this study, we measured the shape-properties, groundwater flow, and erosion rates over short (hours) and long (tens of thousands of years) timescales in the headwater channels of steep, mountain rivers in a tropical rainforest in Puerto Rico. We identified a distinctive population of streams with geometric properties and stream flow-to-erosion rate relationship that match predictions for channels carved by water flowing underground on both short and long timescales. This is the first study investigating groundwater-driven erosion using ^{10}Be as a direct geochemical tracer.

1. Introduction

Water emerging from the subsurface contributes to landscape evolution, but the evidence of such contribution is often subtle. Seeps enhance chemical weathering, slope toe undercutting, slope failure, and in some cases, stream incision. Horton overland flow, saturation overland flow, and subsurface flow erode the landscape in distinct ways, generating landforms with different characteristics. Channels initiated by overland flow are tightly V-shaped in plan view, tapering towards their head into sharply narrow channels (Carson & Kirkby, 1972; Howard, 1994). Subsurface flow drives sapping erosion (Dunne, 1980), producing broad, shallow incisions that are U-shaped in plan view (Howard, 1994). Connecting form to process, U-shaped channels in Martian topography have been attributed to seepage erosion, implying flowing subsurface water (Baker et al., 1983; Malin & Carr, 1999; Sharp & Malin, 1975). However, as other erosion processes may

generate broad, shallow slope failures the form itself is not diagnostic. Amphitheater-headed channels have been found in landscapes shaped by plunge-pool erosion (Lamb et al., 2006, 2007) and by cliff collapse (Weissel & Seidl, 1997) in addition to by sapping and seepage erosion (Higgins, 1982; Laity & Malin, 1985). To date, physical modeling (Howard, 1995) and field studies (Abrams et al., 2009) have connected the process of seepage erosion to incising channels with the amphitheater form under rare conditions, such as uniform substrate with high permeability and infiltration capacity in excess of normal precipitation.

Groundwater sapping is the intermittent collapse of an escarpment due to undercutting above a seep. Undercutting increases the hydraulic gradient of the water table, and thereby accelerates groundwater fluxes to the seep point. As a result, flow lines in the subsurface converge toward the backwearing seep wall, expanding the size of the underground area that feeds the seep (Dunne, 1980). Howard et al. (1988) developed a numerical model describing seepage erosion in cohesionless sediment which he tested through a series of sandbox experiments. He identified specific areas where sapping or fluvial erosion dominate. The sapping zone is located near the base of the escarpment; it is a region where sediment delivered by cliff collapse piles-up near the angle of repose before being periodically entrained farther down the stream network by discharged groundwater. Downstream of the sapping zone, the deposited material is slowly winnowed away by baseflow in the fluvial zone, if discharge is capable of transporting the sediment. The model predicts that erosion rate is proportional to groundwater influx at the channel head. Abrams et al. (2009) tested this model on a network of steep-head channels located in the Apalachicola River, on the Florida panhandle. They found a linear relationship between channel headwall backwearing rate and contributing drainage area for the channel network.

Linear scaling between stream incision and discharge/drainage area is a distinctive characteristic of channels that grow by seepage erosion and groundwater efflux. Indeed, incision by streams fed by surface runoff tends to follow a power law function of drainage area and channel steepness (stream power model). Neither model explicitly includes grain size and channel width as variables, both of which impact erosion (Lague, 2014; Sklar & Dietrich, 1998). Groundwater sapping models, however, tend to treat the downstream transition from sapping to fluvial transport as a continuum (Dunne, 1988; Howard & Mclane, 1988; Kochel et al., 1985). In doing so, they implicitly require that groundwater discharge be sufficient to transport particles away from the seepage face. The low velocity of groundwater is regarded as insufficient to transport coarse grained material in most settings (Lamb et al., 2006), requiring contribution of overland flow.

The importance of groundwater flow in the hydrology of the Luquillo Experimental Forest (LEF) of northeastern Puerto Rico is well established owing to decades of research (Bhatt & McDowell, 2007; Chestnut & McDowell, 2000; Derry et al., 2006; Kurtz et al., 2011; Murphy & Stallard, 2012; Scholl et al., 2015; Shanley et al., 2011; Stallard, 2012b). However, its contribution to the geomorphic evolution of the landscape has not been addressed. Our objective in this work is to determine whether seepage erosion contributes to the growth of the Rio Blanco stream network through expansion of the headwaters. We surveyed ~200 springs feeding first order channels, in a part of the LEF underlain by slowly eroding quartz diorite, mantled by a thick saprolite. These springs are often located in amphitheater-shaped, hemispheric valley heads. Unlike studies of bedrock stream incision by groundwater (e.g., Hawaii and the Colorado Plateau; Kochel & Piper, 1986; Laity & Malin, 1985; Lamb et al., 2007), our investigation finds evidence for widening of valley head features by sapping and sediment transport in first order drainages under baseflow discharge. The study area possesses several characteristics that are favorable to seepage erosion, including overall shallow gradient streams, low-cohesion subsurface material, and a continual, high rate of groundwater recharge. As a first line of evidence, we compare the geometric properties of channel heads in this river network to the predicted amphitheater-shape that is a characteristic of groundwater erosion (Dunne, 1980; Howard et al., 1988; Petroff et al., 2011). A criticism of many studies that attribute U-shaped channels to groundwater is that the low velocity of baseflow is incapable of transporting material in the channel. We measured the bedload flux of material under baseflow, documenting the transport capacity of subsurface water discharged into the channels. Further, we measured catchment-averaged erosion rates in a group of amphitheater-shaped channels using *in situ*-produced ^{10}Be from the bedload sediment and found that despite small contributing drainage areas, these channel tips are exporting sediment at rates that are generally higher than the range of ridgetop erosion rates (25–50 m/My) determined by prior research for this study

area (Brown et al., 1995). The mismatch in erosion rates indicates a deepening valley network but contains no information about erosion mechanisms. Hydrograph analyses in our study area show that flash floods occur frequently (Murphy & Stallard, 2012; Stallard, 2012a), with an early and significant contribution of groundwater to the peak discharge (Kurtz et al., 2011), so channel heads incised by sapping could depend on high discharge events that clear sediment away from the seep face and out of the stream channel (Gellis, 2013; Murphy & Stallard, 2012), which would result in higher erosion rates than expected from base-flow groundwater discharge alone.

1.1. Field Setting

The Luquillo Mountains are located in northeastern Puerto Rico (Figure 1) and represent the first topographic barrier encountered by the Westerly trade winds (Scatena & Larsen, 1991). Consequently, orographic forcing makes this area the wettest region in Puerto Rico, with mean annual precipitation ranging from 2.5 m/y at the coast to 4.5 m/y at the peaks (Figure 1; García-Martinó et al., 1996; Murphy et al., 2017). Although hurricanes and tropical storms provide the highest intensity rainfall events, most precipitation is delivered by low-intensity rainfall (Brown et al., 1983; Murphey & Stallard, 2012). The study area encompasses the upper Rio Blanco watershed, which drains the southern flank of the Luquillo Mountains. While stream discharge and chemistry have been well studied, the shape of the water table, as well as the volume of water stored in the saprolite and underlying fractured aquifer, remains poorly constrained, due to the pristine nature of the old-growth forest, its remoteness, and its protection status. By inventorying the springs that are still flowing at base flow, as well as numerous small incisions that go dry, we obtained the first spatially extensive dataset of local water table position in the study area. It suggests the presence of a large, persistent aquifer. This inference is in agreement with long-term hydrological monitoring of Rio Icacos, demonstrating a sustained baseflow component contributes ~75% of the total river discharge (Chestnut & McDowell, 2000; Scholl et al., 2015; Shanley et al., 2011).

The material composition in the subsurface is a strong control on the volume, flow paths, and residence time of groundwater. As explored by Dunne (1980, 1990) compositional heterogeneities, fractures, openings and pore networks influence the flow field, potentially overriding the influence of topographic curvature on flow

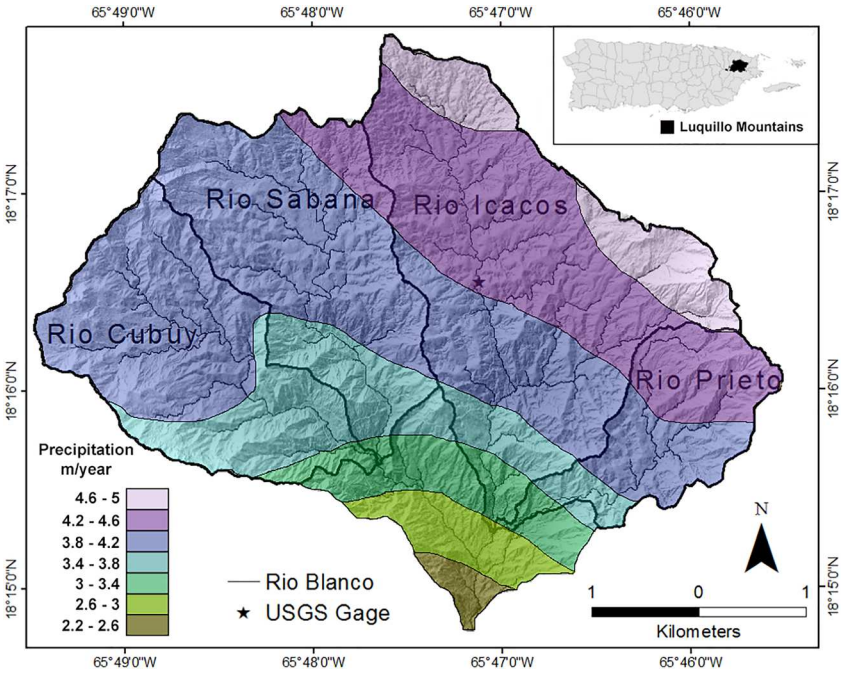

Figure 1. Map of the Rio Blanco watershed with the four main tributary rivers identified: Rio Cubuy, Rio Sabana, Rio Icacos, and Rio Prieto. The color gradient corresponds to the orographic precipitation gradient. Rainfall quantities and patterns were reported by Murphy et al. (2017). USGS gage 50075000 is marked with a black star symbol. In the upper right-hand corner is an inset map showing the island of Puerto Rico with the area of the Luquillo Mountains in black.

line convergence at seep locations. Weathering has broken down the rock material at depths well below the emergence of spring waters. Thick profiles of intensely weathered saprolite overlay the bedrock and extend for tens of meters into the subsurface (Buss et al., 2013). The bedrock weathers along fracture planes into spheroidal corestones (Buss et al., 2008, 2013), which are exhumed along drainage lines but rarely crop out on hillslopes. The physical and hydraulic properties of the saprolite indicate that it is capable of absorbing and storing large quantities of water. Porosity values of ~45% are constant with depth (White et al., 1998), and dry bulk density averages 0.75 g cm^{-3} (Larsen et al., 1999). Infiltration rates are highest in near surface soils, exceeding all but the greatest rainfall intensities for the area (Larsen et al., 1999). Piezometer studies have found that groundwater recharge during storms is linked to slope failures occurring 12–96 hr after the storm event (Simon et al., 1990). However, storm-generated precipitation also moves through the shallow subsurface as quickflow (Kurtz et al., 2011) leading to shallow slope failures that initiate at permeability boundaries where clay horizons accumulate (Simon et al., 1990).

2. Methods

2.1. Field campaigns and digital terrain analysis

We located potential springs in hemispheric valleys on a 1 m-resolution lidar digital elevation model (DEM; Luquillo CZO Rio Blanco and Rio Mameyes LiDAR Survey, 2010–2011) and verified the presence of flowing water in field campaigns. From the digital map, we measured the width of valley incisions at multiple intervals between the crest of the headwall to the junction with the larger river network to compare with the prediction of continually spaced, rather than widening, channel valleys (Figure 2a). We note that these measurements correspond to the valley incision and not the wetted channel. Petroff et al. (2011) defined the plan form aspect ratio of a channel head as the ratio between the valley width and the radius of a circle fitted to the tip of the incising channel (Figure 2c). We calculated comparable metrics for a subset of the seeps we surveyed ($n = 99$). In order to define the location of the circle fit to the channel tip, we pulled longitudinal profiles from the DEM and identified the slope-break occurring at seep point and the start of channelized flow. The seep point and channelized flow do not always correspond in space due to deposition caused by sapping at the seep (Figure 2b).

We measured catchment-averaged erosion rates for five of the amphitheater-shaped channels, and at these sites, we calculated the k_{sn} for the channels using Topo Toolbox in Matlab (Schwanghart & Scherler, 2014) and defined an average slope from that value, using the equation

$$S = Ksn^{*}A^{-\frac{m}{n}}. \quad (1)$$

We set $m = \frac{1}{3}$ and $n = \frac{2}{3}$ for the calculation, values which are typical for steady-state stream channels (Whipple & Tucker, 1999), an appropriate assumption for these low-gradient, concave-up streams.

2.2. Baseflow discharge measurements

Baseflow is the fraction of river discharge that comes from groundwater storage (Hall, 1968). Long-term monitoring of Rio Icacos has shown that baseflow forms a significant portion of river discharge (~75%; Derry et al., 2006; Kurtz et al., 2011; Schellekens et al., 2000, 2004; Scholl et al., 2015; Shanley et al., 2011). During low flow conditions, nearly all of the discharge in the small, sandy channels forming from the coalescence of seeps are therefore contributed by groundwater. During our field campaign in June of 2016, the Luquillo Mountains had not received high-intensity rainfall for nearly 2 weeks. Sampling was completed between 14 June 2016 and 18 June 2016. Discharge measured at the USGS gage on Rio Icacos for the entire time period of sampling averaged 10.1 L/s with a standard deviation of 0.5 L/s. We measured baseflow discharge using salt plug tracer injection (Moore, 2004a, 2004b) in five seep-formed channels, and weirs in an additional two where channel reaches were too short to apply the tracer method (Figure 3). Measurements were made as close as was practical to the initiation point of channelized flow, that is, typically, no more than a few meters from the channel head.

The size of this data set was constrained by complexities of the field setting, especially by the small size of the seep channels. In order to estimate baseflow discharge at these smaller channel sites, we used an empirical relationship between baseflow rate and drainage area for the watershed. We supplemented discharge

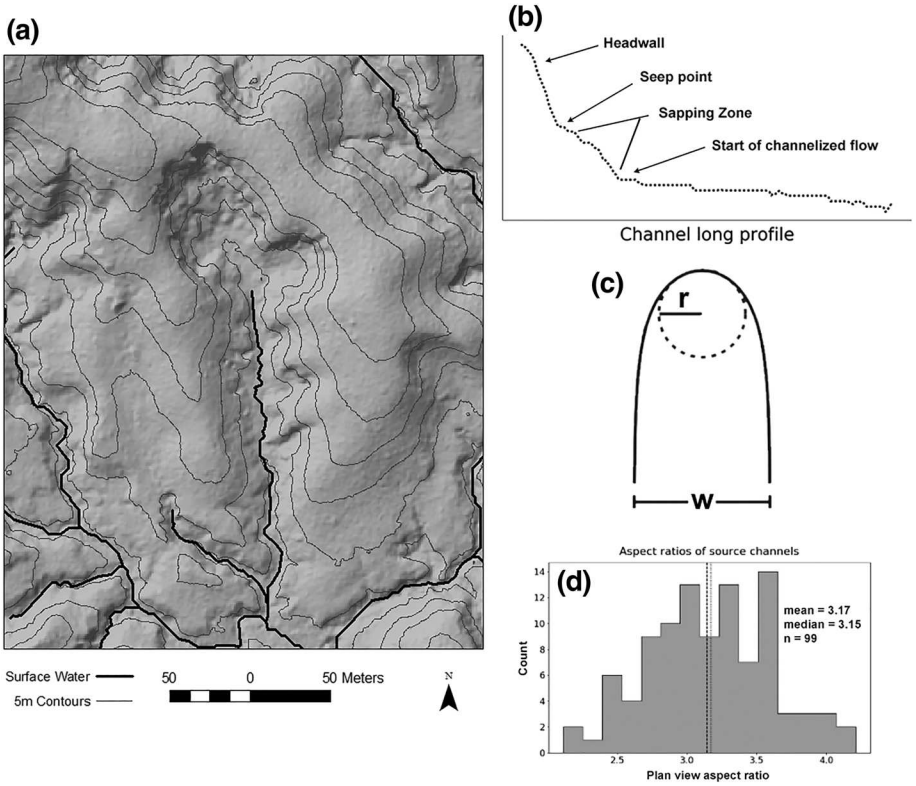

Figure 2. (a) Shaded contour map of a seep-fed, amphitheater-shaped channel in Rio Icacos. Baseflow discharge and long-term erosion rate were both measured at this site. (b) Long profile of the channel pictured in 2a derived from a 1 m DEM. Foci of sapping erosion and fluvial transport are identified, following the morphology of seepage eroded channels described by Howard (1995). (c) Diagram adapted from Petroff et al. (2011) showing the measurements of planform aspect ratio of channel head features. (d) Measurements of plan view aspect ratio for 99 amphitheater-shaped channels. Mean of the measurements is 3.17, and median is 3.15.

measurements from seeps with additional measurements of baseflow in larger subcatchments using the same salt-plug tracer injection ($n = 6$) and the discharge recorded for Rio Icacos at USGS stream gage 50075000 (Figure 3). The measured catchments have a range of drainage areas (0.0008–4.1 km^2), which were extracted from the 1 m-resolution lidar assuming that surface and underground watersheds coincide. Mean annual rainfall increases from 3.8 to 4.6 m/y across the study area (Murphy et al., 2017, Figure 1). We therefore weighted drainage area by the precipitation average across each individual catchment. We combined measured discharge and precipitation-weighted drainage area to construct a linear discharge-to-drainage area model for the studied group of seeps and fluvial catchments (11 in total). We improved the robustness of the linear fit to the data through 1,000 bootstrapped iterations of the measured data points. We used this field-calibrated relationship to calculate baseflow discharge in other channels based on their precipitation-weighted drainage area.

2.3. Bedload grain size and mobility

At one amphitheater-headed channel, we deployed a Helley-Smith bedload sampler (Emmett, 1980) for 3 hr and 15 min under baseflow conditions (discharge of 0.94 L/s) to catch the mobile bedload (Figure 3). The sample was sieved into phi-scale size fractions (<0.063, 0.063–0.125, 0.125–0.25, 0.25–0.5, 0.5–2 mm diameter). The cumulative sum of the size fractions was used to determine the D_{50} of the bedload sample.

2.4. Catchment-averaged detrital ^{10}Be erosion rates

We collected grab samples of in-stream sediment from five amphitheater-headed channels at the start of channelized flow, proximal to the incised tip (Figure 3). We quantified the accumulation of *in situ*-produced ^{10}Be in river borne quartz during its exhumation and transportation off the slopes draining to these channels

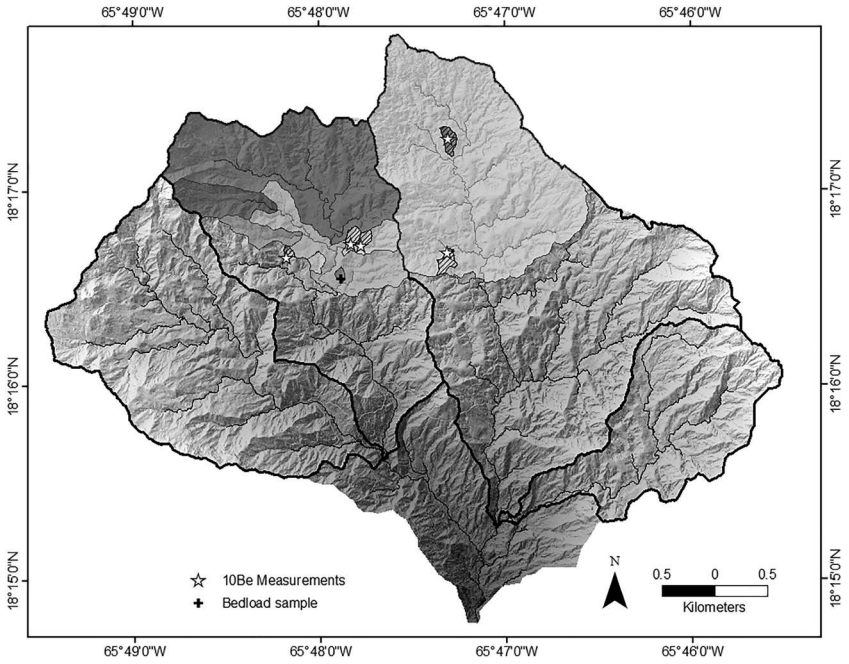

Figure 3. Map of the Rio Blanco watershed with sampling sites for this study identified. Baseflow discharge rates were measured for each of the watersheds identified by shading. Sediment collected from stream channels and measured for ^{10}Be concentrations are identified in white star symbols, and the contributing drainage area for those measurements is identified with a black line pattern. The black cross symbol marks the location where sediment moving as bedload in a stream at baseflow was collected.

(Brown et al., 1995; Granger et al., 1996). ^{10}Be is produced in the mineral lattice of quartz grains in the upper ~2 m of Earth's surface at a well-constrained rate (Dunai, 2010; Gosse & Phillips, 2001; Lal, 1991). In many settings, ^{10}Be records the total volume of mass lost from chemical and physical erosion (Dixon & Riebe, 2014)—but here, saprolite production and chemical weathering occur at depths greater than the average attenuation length (Buss et al., 2013), such that ^{10}Be mostly documents physical erosion (Dixon & von Blanckenburg, 2012). In-stream collection assumes that a random sample of material actively transported by a stream represents an average of the landscape contributions above the collection site (Bierman & Nichols, 2004; Brown et al., 1995; Granger et al., 1996).

Samples were prepared in the Scripps Cosmogenic Isotope Laboratory, University of California San Diego. The sieved 0.25–0.5 mm sand fraction was purified until only etched quartz remained, following an adaptation of the technique developed by Kohl and Nishiizumi (1992). A ^{9}Be carrier (Supplier Purdue Rare Isotope Measurement Laboratory, Designation 2017.11.17-Be) was added to each sample prior to quartz dissolution in hot, hydrofluoric acid. We separated Be from other elements following von Blanckenburg (2004). We oxidized the samples over a flame to convert the BeOH to BeO, added niobium powder to the BeO powder, then packed the samples into a cathode target. The ^{10}Be/^{9}Be ratio of the samples was measured by accelerator mass spectrometry at PRIME Laboratory, Purdue University. Results were normalized to the 07KNSTD standard (Nishiizumi et al., 2007) with a ^{10}Be/^{9}Be ratio of 2.79×10^{-11} (Balco et al., 2009).

We calculated catchment average erosion (ε) from the ^{10}Be concentrations of the samples using equation 2 (Dunai, 2010; Lal, 1991), where $P(z)$ is the shielding corrected production rate, $C(z)$ is the nuclide concentration, λ is the ^{10}Be decay constant, Λ is the attenuation length, and ρ_s is the material density.

$$\varepsilon = \left(\frac{P(z)}{C(z)} - \lambda\right) * \frac{\Lambda}{\rho_s}. \quad (2)$$

For this calculation, we assign a material density of 1.6 g cm^{-3} and calculate a ^{10}Be production rate with the CRONUS calculator from the latitude, longitude, and elevation of sampling locations and an assigned

shielding correction (Balco et al., 2008). Shielding corrections assume vegetative shielding (7%, details in Brocard et al., 2015) and invariant bedrock composition within the catchment feeding area (geologic map in Brocard et al., 2016).

The ^{10}Be concentration in river born sediments integrates the entire upstream drainage area, thus deriving an average for the contributing catchment. In this study, we restrict our results as nearly as possible to the erosion rate at the channel head by sampling at the initiation point of channelized flow to reduce ridgeline contributions to the sediment flux. The channel head topography is a conical depression, which results in a complex shielding geometry (Codilean, 2006). However, as demonstrated by DiBiase (2018), oblique radiation on sloping surfaces increases the effective vertical attenuation length in the subsurface such that, except in the most rugged topographic settings, no topographic shielding correction factor is required for catchment-averaged erosion rates at sites where the lithology and surface erosion are spatially constant.

3. Results

3.1. Field campaigns and digital terrain analysis

The headwaters of Río Blanco host numerous springs ($n = 254$) although the smallest are not constantly flowing. Although most springs are not associated with any specific erosional landforms, a sizable population ($n = 99$) lie beneath semicircular, steep valley headwalls that show evidence of slumping (Figure 4a). Seeps surge from saprolite, 4–40 m below the ridge crests that enclose the valley heads, below surface soils in general, and below the clay Bt horizon in particular. Clay accumulation horizons create permeability transitions that concentrate flow (quickflow) in the vadose zone during storms and have been linked to shallow slope failures typically seeded at depths ~0.5 m (Simon et al., 1990). Headwall failures above seep points initiate well below clay horizons where there is no contrast in the material permeability. In addition, seep flow is not fed by quickflow, which corresponds to the fraction of subsurface flow that occurs in the highly permeable soil above the Bt. Therefore, the slumping process carving the amphitheater-shaped headwalls is not primarily driven by excess flow during storm events or at permeability contrasts. Immediately downstream of the seeps, water flow is not channeled, and overland flow takes place over a sandy substrate for a short distance before concentrating into small streams with cohesive banks composed of soft sediment (Figure 4b). Bank cohesion may be aided but is not necessarily armored, by the presence of roots. Channel beds are sandy, with well-developed ripples and bars (Figure 4c).

We recorded many seeps associated with amphitheater-shaped valleys ($n = 99$) and measured topographic watershed areas spanning three orders of magnitude (0.0008–0.03 km^2) contributing drainage. At each of these sites, we measured the average width of the incised valley walls using a consistent contour interval and the radius of a circle fit to the incision at the point of seep emergence, following methods described in Petroff et al. (2011). The average channel planform aspect ratio (width/tip radius) for the population is 3.17, and the median is 3.15, which matches the predicted aspect ratio for channel morphologies associated

Figure 4. (a) Image of the channel headwall and unchannelized flow from the seep. (b) Seep waters saturate piles of sediment at the base of headwalls where they emerge from the subsurface. (c) Seep waters forming a channel with well-defined banks.

with sapping erosion (Petroff et al., 2011). All measurements are available in an online supplementary resource using the link in the acknowledgements section.

Channel metrics for five amphitheater-shaped channels are presented in Table 1. Measurements are reported for these channels because we measured the long-term erosion rates for these catchments using ^{10}Be. This subpopulation of amphitheater-shaped channels falls at the larger end of the drainage area distribution for the entire study area—however, based on our observations, the low values measured for channel slope and steepness are consistent with the greater population.

3.2. Baseflow discharge measurements

The slope of linear regression between drainage area and discharge is the mean of 1,000 linear regressions by random iterative sampling on measurements (nine out of 11) giving an r^2 value of 0.86. Residuals are reported in Figure 5. The linear regression was used to calculate discharge of 99 seep-fed channels based on their drainage area. Nonlinear regressions provided higher r^2 values or more normally distributed residuals. However, most of the seeps for which discharge was predicted are seeps where the flow was too low to be reliably measured in the field, and the predictions of nonlinear regressions were poorly constrained at low discharges. Predicted discharge rates at seep-fed channels range from 0.04 to 4.4 L/s. These values are comparable to groundwater discharge (1.1–1.9 L/s) measured in wells along the riparian zone of a small second-order tributary by Chestnut and McDowell (2000).

3.3. Bedload grain size

The D_{50} of the bedload sample, a medium sand size between 0.25 and 0.5 mm (Figure 6), is similar to the median size of quartz grains in the saprolite (White et al., 1998). No grains larger than 2 mm were collected during the sampling or observed in either the channel reach, the sapping zone, or the headwalls of the amphitheater-shaped channels.

3.4. ^{10}Be catchment erosion rates

Catchment-averaged erosion rate measurements were made in watershed drainages spanning an order of magnitude in area (0.003–0.039 km^2; Table 2). Samples were collected in the headwaters of two main branches of Río Blanco: Río Icacos and Rio Sabana (Figure 1). ^{10}Be concentrations ranged between 88 and 287 $\times$ 10^3 at/g. Four procedural blanks ran with the samples had ^{10}Be/^{9}Be ratios between 3.5 and 5 $\times$ 10^{-15}. Measurements yield erosion rates between 40 $\pm$ 3 and 130 $\pm$ 10 m/My.

4. Discussion

Structurally, the hemispheric headwalls of the amphitheater channels in Rio Blanco suggest formation by subsurface flow dynamics akin to those outlined by Dunne (1980), 1990) and generalized by Petroff et al. (2011). Field evidence supports headwall erosion by sapping, rather than overland flow or shallow landslides (Lamb et al., 2006, 2007; Simon et al., 1990), which leads us to attribute the shape properties of these channels to seepage erosion. Of itself, this implies diffusive subsurface flow through a substrate where there are spatially nonuniform material properties (e.g., corestones, a clay horizon, root voids). We propose that a deepening chemical erosion front has entrenched the local water table within a zone of thick, highly weathered saprolite in which the subsurface flow field is relatively unimpacted by such heterogeneities.

Table 1
Channel Metrics Extracted From 1 m DEM

Site ID	Migration distance (m)	Incision depth (m)	k_{sn}	% Slope[a]	Drainage area (m^2)
IC-GW1	120	84	6	3.8	82450
IC-GW2	250	40	2	1.2	27150
Sab-GW8	87	48	2	1.5	11495
Sab-GW9	112	50	4	3.3	10079
Sab-GW16	160	50	3	3.2	38882

[a]Calculated from k_{sn} value and equation 1 using values $m = \frac{1}{3}$ and $n = \frac{2}{3}$.

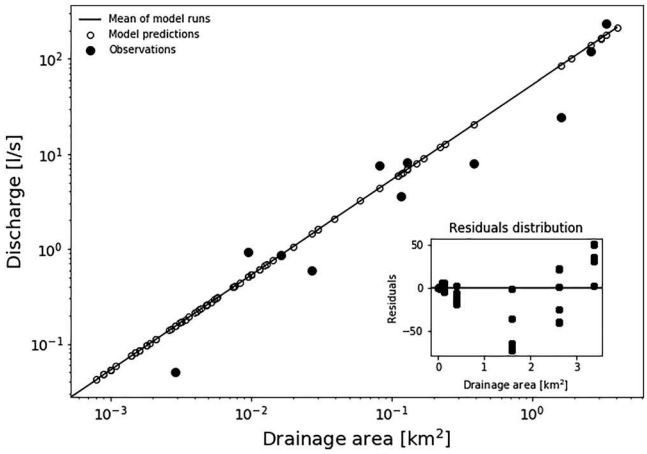

Figure 5. A linear model with the equation $y = 53.06x$ relating the contributing drainage area to the baseflow discharge rate. Baseflow measurements made in the field for 11 subcatchments with a range of contributing drainage areas. The black line represents the average outcome of iterative random resampling of the data and is the model prediction of the relationship between drainage area and discharge. The drainage areas of 99 additional catchments are plotted along the line showing the model-predicted range in baseflow discharge rate for seep-fed channels within the Rio Blanco. Residual distribution of the model is plotted in the bottom right inset.

Expansion of the stream network via sapping and seepage erosion requires that subsurface discharge must be forcible enough to erode the material deposited in the sapping zone and in-channel sediment. As pointed out by Lamb et al. (2006), seepage erosion is shut off if discharge from the seep is incapable of transporting coarse grained material away from the face. As such, the linear relationship between discharge and erosion in seepage-carved channels proposed by Howard (1995) has been evaluated thus far in just one natural setting on the Florida panhandle (Abrams et al., 2009). In the discussion that follows, we evaluate the applicability of Howard's model using a direct geochemical tracer of erosion for the first time.

4.1. Distribution of spring-fed channels

Amphitheater-shaped channels are concentrated in the upland portion of the watershed (Figure 7) and cluster in the interior of stream basins, away from the drainage-divide forming ridges that separate the four principal tributaries. We attribute this distribution of amphitheater-type channels to a combination of greater precipitation at higher elevations (Murphy et al., 2017) and spatial patterns in the inferred depth to solid bedrock. The upland reaches of these tributary watersheds are bowl-like, with lower relief-topography surrounding the river channel (Comas et al., 2018). Ridgelines in this section of the watershed have the slowest documented erosion for the entire catchment (25–50 m/My; Brocard et al., 2015, 2016), and thick, highly depleted weathering profiles (Buss et al., 2013; Porder et al., 2015). In quickly eroding parts of the watershed, all of the springs we observed feed into nonhemispheric V-shaped channels with steep, boulder-choked heads.

An erosive wave traveling up the Rio Blanco watershed generated sharp knickpoints that separate the landscape into a slowly eroding upper catchment and a steep lower catchment eroding twice as fast (Brocard et al., 2015, 2016). The furthest extent of knickpoint propagation, mapped in Brocard et al. (2015, 2016) is indicated in the topography ("Erosion Front," Figure 7). In a study by Comas et al. (2018) utilizing geophysical methods to visualize the deep critical zone architecture, the authors suggest that upstream of the erosion front the depth to fresh rock is significantly greater. There are no amphitheater-shaped channels in the topography downstream of the erosion front, and we observed few springs emerging overall. The absence of springs may be due to decreased porewater as the saprolite layer thins. Furthermore, fast erosion enhances core stone exhumation, as evidenced by the number of in-channel boulders in stream reaches adjusting to the modern base level (Pike et al., 2010).

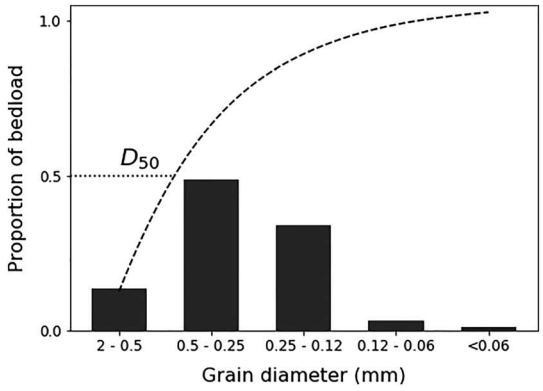

Figure 6. Material mobilized under baseflow in a seep-fed channel, collected with a bedload sampler. Representative portion of size fractions plotted as a histogram, line plot showing the cumulative function of the size fractions. D_{50} is the median value of the cumulative function.

We do not attempt to isolate the contribution of seepage erosion to channels where core stones have accumulated. Channel armoring by coarse material would shut off sediment transport at baseflow discharge. The focus of this study is the multistep process of headwall sapping supplying sediment to the valley bottom, and the progressive transport of that material by baseflow into the greater fluvial network. At some sites, we observed pipes excavated at the edges of core stones, likely due to concentrated subsurface flow, as described by Dunne (1990). This type of seepage erosion may contribute to the total sediment exported in the watershed. However, it is distinct from rotational slumping at channel heads that is caused by saturation in the saprolite.

4.2. Landscape (dis)equilibrium and stream incision

Multiple methods document nonuniform erosion across the upstream landscape, characterized by faster erosion along hillslopes than on

Table 2
Cosmogenic ^{10}Be-Derived Erosion Rates

Site ID	Lat	Long	Elevation (m)	Shield corr.	[^{10}Be][a] (atoms/g)	AMS Uncert. (atoms/g) %	Prod. rate (spall)	Erosion rate (m/My)	Rate Uncert. (m/My)
IC-GW2	−65.7884	18.2875	623	0.98	13,4983	4,623 3.4%	9.66	84.96	±7.16
IC-GW1	−65.7884	18.2878	629	0.98	88,491	1,380 1.6%	9.71	131.43	±10.2
Sab-GW8	−65.7971	18.2786	651	0.98	287,067	5,574 1.8%	9.91	40.01	±3.25
Sab-GW9	−65.7962	18.2786	655	0.98	268,924	4,367 1.6%	9.95	42.96	±3.45
Sab-GW16	−65.8029	18.2777	643	0.98	185,315	3,454 1.9%	9.84	62.43	±4.99

[a]The measured ratio of the carrier yielded a ^{10}Be/^{9}Be ratio of $0.5 \pm 0.1 \times 10^{-15}$.

ridgelines. The ^{10}Be erosion rates that we measured in amphitheater channels (Table 2) span a range comparable to the differences in erosion rates between the slowly eroding upper landscape and the faster-eroding downstream landscape (Brocard et al., 2015). This difference, and the propagation of this wave of incision across the Río Blanco catchment, is driven by the lowering of the general base level of Río Blanco. However, the differences in erosion upstream of the front of erosion are not driven by a drop in base level, since little lowering occurs along the main streams. The four major streams draining the Río Blanco catchment have low gradients and are alluvium-bedded in their headwaters. They become steep bedrock rivers after passing the front of erosion. The alluvial reaches are graded to bedrock sills located in the riverbeds at the front of erosion, which act as a local, perched base level. Headward propagation of the front of erosion is slow (~1 mm/ky, Brocard et al., 2016). The bedrock sills provide a relatively stable base level for the alluviated reaches.

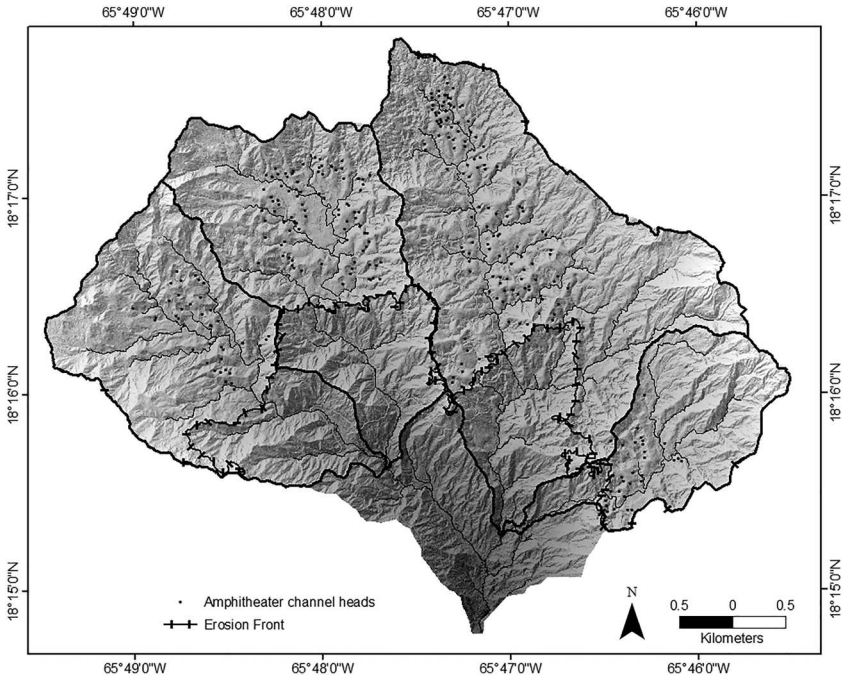

Figure 7. Locations of semicircular channel heads (black dots) within the Rio Blanco catchment. The boundaries of the four major tributary rivers are identified by thick black lines. A dashed black line indicates the extent of knickpoint retreat up the river channels and the front of the erosive wave impacting the hillslopes (Brocard et al., 2015, 2016).

In the absence of regional base level as a driver, what process causes the differentiation of stream and ridge erosion? Valleys may deepen due to top-down differences in erosion (i.e., induced by vegetation or rainfall gradients) or bottom-up by base-level change. Mountain uplift would have increased the orographic effect, but the persistence of a protective vegetative cover and the slow rate of knickpoint advance has maintained overall low erosion rates in the upland topography. It is possible that the combined effect has deepened the solid-rock interface and induced lowering of a local base level set by the subsurface water-routing system. Brown et al. (1995) proposed differentiation between hillslope and stream erosion rates began 1.3 Ma in Rio Icacos from measurements of ^{10}Be-derived erosion rates in the fine fraction of river sediments. There is a strong grain-size dependence in ^{10}Be-derived erosion rates in the Rio Blanco, which has been interpreted to reflect landsliding that delivers grains shielded at depth directly to the channel. Using the coarse sediment fraction, differentiation between ridgelines and channels initiated 110 ky ago (Brocard et al., 2016). The initial uplift of the Luquillo Mountains dated by Brocard et al. (2015) occurred 4.4 Ma, providing an upper age constraint for valley deepening.

We estimated the initiation age of valley incisions as the time required to erode a volume of sediment that would fill the existing valley incision (Table 3). The rate of excavation was derived from the ^{10}Be erosion rates, and the approximate volume of excavated sediment was calculated from the DEM. Eroded volume was calculated as the valley surface area (m^2) multiplied by the depth of the incision between the ridge crest and seep point at the valley headwall (m; Figure 2b). This volume is an underestimate due to the elevation lost between the seep emergence point and the river junction downstream. Stream incision commenced between 500 ky and 1.2 Ma following this approximation. This timeframe may represent the moment when the saprolite had deepened sufficiently to induce seepage erosion following mountain uplift. We only infer this process for the population of small, amphitheater-shaped channels that are mapped in Figure 7—and recognize that other processes likely form larger, more complex catchments in the watershed.

4.3. Stream incision models

Howard et al. (1988) proposed that the incision rate of seep-eroded channels is linearly proportional to the discharge of water at the seeps. Abrams et al. (2009) showed that this model is consistent with the morphology of a channel network incised into fluviodeltaic and marine sediments in the Apalachicola delta, Florida. Channel erodibility is an empirically derived proportionality coefficient in this and other stream incision models. In this field setting, the channel is incising low-cohesion sediment; therefore, a transport coefficient is more appropriate than an erodibility constant.

To analyze the performance of the Howard (1995) model over our field area, we compared baseflow discharge to our catchment-averaged ^{10}Be soil erosion rates, integrated over 10^3–10^4 years (Figure 8, data compiled in Table 4). Long-term incision rates correlate linearly with baseflow discharge rates ($r^2 = 0.87$), suggesting that seepage erosion, rather than surface flow, drives the erosion of the valley heads. We repeat this analysis on data from streams in the same watershed that drain V-shaped, core-stone choked source points (data from Brocard et al., 2016), where we expect a weaker coupling between baseflow and erosion (Figure 8 inset). No scaling between baseflow discharge and erosion rate is found among the dataset of core-stone choked stream catchments ($r^2 = 0.18$), the erosion of which is therefore not properly described by ground seepage. The baseflow discharge rate we model is based on catchment drainage area, and a multi-site compilation of V-shaped channels found no trend between ^{10}Be erosion rates and drainage area (Schaller et al., 2001), suggesting the scaling shown here is not an artefact of the ^{10}Be method. However, this relationship does not

Table 3
Estimated Initiation Age of Incision

Site ID	^{10}Be-derived erosion rate (m/My)	Estimated eroded volume (km^3)	Approximate initiation age (Ma)
IC-GW1	131 ± 2.1	6.93	0.6
IC-GW2	85 ± 2.9	1.086	0.5
Sab-GW8	40 ± 0.8	0.552	1.2
Sab-GW9	43 ± 0.7	0.504	1.2
Sab-GW16	62 ± 1.2	1.944	0.8

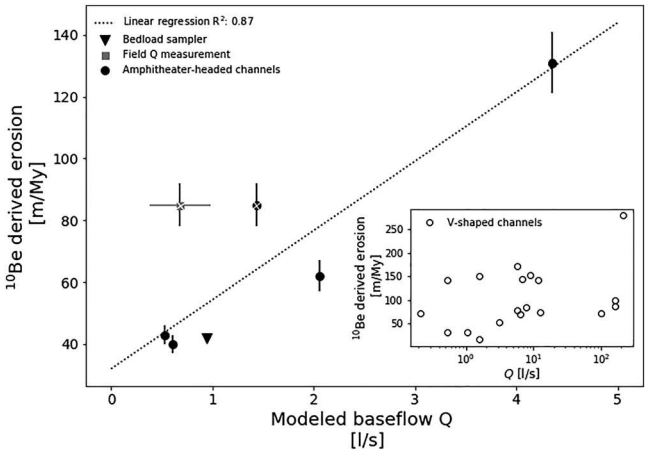

Figure 8. Long-term (10^3–10^4 y) ^{10}Be-derived catchment-averaged erosion rates as a function baseflow discharge for five seep-fed channels. Baseflow discharge rates were calculated using the field-calibrated relationship between drainage area and discharge (Figure 5). Dotted line: linear regression ($r^2 = 0.86$). Solid square: seep-fed channel for which field-measured discharge is available. The model predicted baseflow discharge rate is greater than the measured value, which is also visible in the residuals plotted for the model results in Figure 5. The corresponding modeled and measured data points have been indicated by white x-marks on the marker faces. Triangle: volumetric baseflow sediment flux converted to an erosion rate assuming net export of sediment, plotted vs. field measured baseflow discharge in the same channel. Inset: ^{10}Be-derived catchment-averaged erosion rate and calculated discharge for 19 river source points which channel heads are choked with core stones (data from Brocard et al., 2016). No significant correlation is found ($r^2 = 0.18$). Inset plots the x-axis in log scale.

allow us to distinguish between groundwater-driven erosion and vadose-zone seepage occurring during storm events.

The perpetuation of bedload entrainment by baseflow over longer timescales should result in backwearing of the channel into the semi-circular valley headwall, spurring hillslope soil erosion, and ultimately affecting catchment-averaged ^{10}Be soil erosion rates. We measured fine- to medium-sized sand particles moving as bedload at baseflow in one small amphitheater-headed catchment. The sampler was deployed for 195 min, and the total mass of sediment collected during sampling was 23.9 g. If the sediment transported in the channel is not replaced by sediment feeding upstream, this transport rate represents an erosion rate of approximately 42 m/My (Table 4). This short-term sediment flux rate is plotted against field-measured base flow discharge in the same channel in Figure 8. Volumetric transport at baseflow from this single data point agrees well with the relationship defined by the long-term rates. While limited, this agreement suggests that the long-term erosion rates reflect the dynamics of baseflow discharge, rather than large interflow discharges that occur during storms.

4.4. Drainage competition

Catchment areas of amphitheater channels in the upland watershed span an order of magnitude. The relationship in Figure 8 implies that seeps with larger feeding areas erode more quickly. This should lead these channels to capture flow from their neighbors producing a positive feedback of larger catchments eroding increasingly faster and eventually pirating smaller basins. Field observations suggest there are many examples of this dynamic in the interior of the Rio Icacos and Rio Sabana watersheds, having the greatest density of hemispheric incisions. For the benefit of a qualitative illustration of this process, Figure 9 shows a magnified image of the topography in the Rio Sabana.

The valley morphology of the tributary network illustrates the channel head shape common to the channels formed by seepage erosion. This form can be visually contrasted with channel head incisions in the steep topography near the divide and downstream of the erosion front. In the center of the image, two amphitheater channels have joined, merging their feeding areas. An adjacent incision has nearly intersected with the active channel of an upstream tributary. The channel in the amphitheater-shaped valley is ~10 m below the elevation of the Sabana tributary channel, indicating that the incision is likely to pirate the fluvial channel once the remaining ridge is breached. This small section of stream demonstrates that the impact of subsurface water discharge on surface topography is such that it may drive avulsions in the fluvial network.

Table 4
Erosion, Discharge, and Drainage Area of Channels in Figure 8

Site ID	^{10}Be-derived erosion rate (m/My)	Drainage area (m^2)	Modeled baseflow Q[a] (L/s)
IC-GW1	131 ± 2.1	82,450	4.4
IC-GW2	85 ± 2.9	27,150	1.45
Sab-GW8	40 ± 0.8	11,495	0.61
Sab-GW9	43 ± 0.7	10,079	0.53
Sab-GW16	62 ± 1.2	38,882	2.08

[a]Derived from the linear model presented in Figure 5.

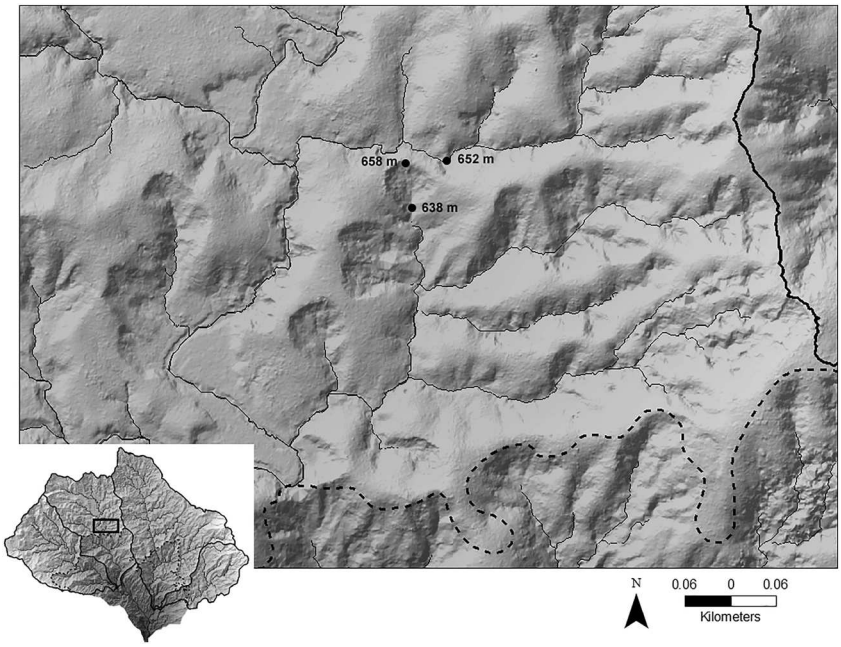

Figure 9. Magnified top-down view of valley topography generated from a 1 m resolution lidar DEM. The thick black line traces the ridge crest divide with Rio Icacos to the east, and the dashed line marks the mapped extent of the erosion front propagation (Brocard et al., 2015, 2016). A thinner black line demarcates the fluvial network. The topographic elevation is indicated at a series of points illustrating a future stream capture event, in which sapping driven incision of a headwall will intersect with a larger tributary channel. Inset shows a view of the Rio Blanco watershed with the area of the visualized subsection highlighted in a black rectangle.

5. Conclusions

In this study, we assess whether the headwater of the Rio Blanco watershed in the Luquillo Mountains, Puerto Rico is expanding due to seepage erosion at the heads of the channel network. A population of hemispheric valleys, incised by slumping at the headwalls, is likely formed by high rates of baseflow over long timescales. This finding for a steep, mountain catchment suggests that seepage erosion may impact geomorphic evolution in other, previously overlooked landscapes having deep weathering profiles and large volumes of groundwater. We found that the baseflow discharge in small, amphitheater-shaped channels transports bedload sediments at a rate consistent with the long-term catchment erosion rates derived from ^{10}Be concentrations. This result suggests that the flow regime occurring most often is a larger determinant in channel characteristics than infrequent large floods (Phillips & Jerolmack, 2016). Both measures of sediment export scale linearly with the drainage area feeding amphitheater-shaped channels, a relationship that is consistent with a model of groundwater-driven channel incision proposed by Howard (1995). We found no similar relationship exists between erosion and baseflow discharge in another population of first-order channels from the same watershed, where coarse-grained material armors the alluviated stream bed. Thus, our field study supports distinct relational forms between discharge rate and channel erosion for stream systems dominated by seepage vs. overland contributions to flow.

Erosion rates in the small amphitheater channels exceed the average surface lowering recorded in ridgetop soils and large catchment areas in the Rio Blanco headwaters, indicating deepening relief at these sites. We propose from the evidence collected in this study that seepage erosion is entrenching the valley network. Our estimates place the onset of incision by this process between 500 ky and 1.2 Ma. Research dating the uplift of the Luquillo Mountains has demonstrated that the upland portions of the Rio Blanco catchment are shielded from an incision wave propagating up the river network (Brocard et al., 2016). We hypothesize that a combination of increased orographic precipitation and low erosion in the relict topography allowed the weathering front to deepen sufficiently to entrench the subsurface water routing network, mechanistically lowering the base level set by the emergence of springs at channel heads in the river network. Broadly, we

suggest that the coevolution of groundwater accommodation space and hydrology is a mechanism for topographic change in relict and postorogenic landscapes.

Acknowledgments
Data and the code for models are available online at https://www.hydroshare.org/resource/4bde564f41c146c68ce2d87a73f71526/. Special thanks to Dr. Jon Lopez and Dr. Michael Lamb for helpful conversations that contributed to the advancement of this research. Thanks are due as well to the LCZO community and to our friends in Naguabo, Puerto Rico. This research was supported by NSF grants 1848637 and 1331841 awarded to Dr. Jane K. Willenbring.

References

Abrams, D. M.,Lobkovsky, A. E.,Petroff, A. P.,Straub, K. M.,McElroy, B.,et al.. (2009). Growth laws for channel networks incised by groundwater flow. *Nature Geoscience*, *2*(3): 193–96. http://doi.org/10.1038/ngeo432

Baker, V. R., Boothroyd, J. C., Carr, M. H., Cutts, J. A., Komar, P. D., Laity, J. E., et al. (1983). Channels and valleys on Mars. *Bulletin of the Geological Society of America*, *94*(9), 1035–1054. https://doi.org/10.1130/0016-7606(1983)94<1035:CAVOM>2.0.CO;2

Balco, G., Briner, J., Finkel, R. C., Rayburn, J. A., Ridge, J. C., & Schaefer, J. M. (2009). Regional beryllium-10 production rate calibration for late-glacial northeastern North America. *Quaternary Geochronology*, *4*(2), 93–107. https://doi.org/10.1016/j.quageo.2008.09.001

Balco, G., Stone, J. O., Lifton, N. A., & Dunai, T. J. (2008). A complete and easily accessible means of calculating surface exposure ages or erosion rates from 10 Be and 26 Al measurements. *Quaternary Geochronology*, *3*, 174–195. https://doi.org/10.1016/j.quageo.2007.12.001

Bhatt, M. P., & McDowell, W. H. (2007). Controls on major solutes within the drainage network of a rapidly weathering tropical watershed. *Water Resources Research.*, *43*, W11402. https://doi.org/10.1029/2007WR005915

Bierman, P. R., & Nichols, K. (2004). Rock To Sediment—Slope To Sea With 10 Be—Rates of Landscape Change. *Annual Review of Earth and Planetary Sciences*, *32*(1), 215–255. https://doi.org/10.1146/annurev.earth.32.101802.120539

Brocard, G. Y., Willenbring, J. K., Miller, T. E., & Scatena, F. N. (2016). Relict landscape resistance to dissection by upstream migrating knickpoints. *Journal of Geophysical Research: Earth Surface*, *121*, 1182–1203. https://doi.org/10.1002/2015JF003678

Brocard, G. Y., Willenbring, J. K., Scatena, F. N., & Johnson, A. H. (2015). Effects of a tectonically-triggered wave of incision on riverine exports and soil mineralogy in the Luquillo Mountains of Puerto Rico. *Applied Geochemistry*, *63*, 586–598. https://doi.org/10.1016/j.apgeochem.2015.04.001

Brown, E. T., Stallard, R. F., Larsen, M. C., Raisbeck, G. M., & Yiou, F. (1995). Denudation rates determined from the accumulation of in situ-produced 10Be in the luquillo experimental forest, Puerto Rico. *Earth and Planetary Science Letters*, *129*(1–4), 193–202. https://doi.org/10.1016/0012-821X(94)00249-X

Brown, S., Lugo, A. E., Silander, S., & Liegel, L. (1983). Research history and opportunities in the Luquillo Experimental Forest. Gen. Tech. Rep. SO-44. New Orleans, LA: US Dept of Agriculture, Forest Service, Southern Forest Experiment Station. 132, 44.

Buss, H. L., Brantley, S. L., Scatena, F. N., Bazilievskaya, E. A., Blum, A., Schulz, M. S., et al. (2013). Probing the deep critical zone beneath the luquillo experimental forest, Puerto Rico. *Earth Surface Processes and Landforms*, *38*(10), 1170–1186. https://doi.org/10.1002/esp.3409

Buss, H. L., Sak, P. B., Webb, S. M., & Brantley, S. L. (2008). Weathering of the Rio Blanco quartz diorite, Luquillo Mountains, Puerto Rico: Coupling oxidation, dissolution, and fracturing. *Geochimica et Cosmochimica Acta*, *72*, 4488–4507. https://doi.org/10.1016/j.gca.2008.06.020

Carson, M. A., & Kirkby, M. J. (1972). *Hilslope form and Process*. Cambridge, UK: Cambridge University Press.

Chestnut, T. J., & McDowell, W. H. (2000). C and N dynamics in the riparian and hyporheic zones of a tropical stream, Luquillo Mountains, Puerto Rico. *Journal of the North American Benthological Society*, *19*(2), 199–214. https://doi.org/10.2307/1468065

Codilean, A. T. (2006). Calculation of the cosmogenic nuclide production topographic shielding scaling factor for large areas using DEMs. *Earth Surface Processes and Landforms*, *31*: 785–794. https://doi.org/10.1002/esp.1336

Comas, X., Wright, W., Hynek, S. A., Fletcher, R. C., Brantley, S. L. (2018). Understanding fracture distribution and its relation to knickpoint evolution in the Rio Icacos watershed (Luquillo Critical Zone Observatory, Puerto Rico) using landscape-scale hydrogeophysics. *Earth Surface Processes and Landforms*, *44*(4), 877-885. https://doi.org/10.1002/esp.4540

Derry, L. A., Pett-Ridge, J. C., Kurtz, A. C., & Troester, J. W. (2006). Ge/Si and 87Sr/86Sr tracers of weathering reactions and hydrologic pathways in a tropical granitoid system. *Journal of Geochemical Exploration*, *88*, 271–274. https://doi.org/10.1016/j.gexplo.2005.08.054

DiBiase, R. A. (2018). Short communication: Increasing vertical attenuation length of cosmogenic nuclide production on steep slopes negates topographic shielding corrections for catchment erosion rates. *Earth Surface Dynamics*, *6*(4), 923–931. https://doi.org/10.5194/esurf-6-923-2018

Dixon, J. L., & Riebe, C. S. (2014). Tracing and pacing soil across slopes. *Elements*, *10*(5), 363–368. https://doi.org/10.2113/gselements.10.5.363

Dixon, J. L., & von Blanckenburg, F. (2012). Soils as pacemakers and limiters of global silicate weathering. *Comptes Rendus - Geoscience*, *344*(11–12), 597–609. https://doi.org/10.1016/j.crte.2012.10.012

Dunai, T. J. (2010). *Cosmogenic nuclides: Principles, concepts and applications in the Earth surface sciences*. Cambridge, UK: Cambridge University Press.

Dunne, T. (1980). Formation and controls of channel networks. *Progress in Physical Geography*, *4*(2), 211–239. https://doi.org/10.1177/030913338000400204

Dunne, T. (1988). Hydrology and mechanics of erosion by subsurface flow. In *Hydrogeology*. Boulder, CO, USA: Geological Society of America, 988.

Dunne, T. (1990). Hydrology mechanics, and geomorphic implications of erosion by subsurface flow. In *Groundwater Geomorphology: The Role of Subsurface Water in Earth-Surface Processes and Landforms*. 1–28.

Emmett, W. W. (1980). A field calibration of the sediment-trapping characteristics of the Helley-Smith bedload sampler. *US Geological Survey, Professional Paper*, *1139*.

García-Martinó, A. R., Warner, G. S., Scatena, F. N., & Civco, D. L. (1996). Rainfall, runoff and elevation relationships in the Luquillo Mountains of Puerto Rico. *Caribbean Journal of Science*, *32*(4), 413–424.

Gellis, A. C. (2013). Factors influencing storm-generated suspended-sediment concentrations and loads in four basins of contrasting land use, humid-tropical Puerto Rico. *Catena*, *104*, 39–57. https://doi.org/10.1016/j.catena.2012.10.018

Gosse, J. C., & Phillips, F. M. (2001). Terrestrial in situ cosmogenic nuclides: Theory and application. *Quaternary Science Reviews*, *20*(14), 1475–1560. https://doi.org/10.1016/S0277-3791(00)00171-2

Granger, D. E., Kirchner, J. W., & Finkel, R. C. (1996). Spatially averaged long-term erosion rates measured from in situ-produced cosmogenic nuclides in alluvial sediment. *The Journal of Geology*, *104*(3), 249–257. https://doi.org/10.1086/629823

Hall, F. R. (1968). Base-flow recessions—A review. *Water Resources Research*, *4*(5): 973–83. http://doi.wiley.com/10.1029/WR004i005p00973

Higgins, C. G. (1982). Drainage systems developed by sapping on Earth and Mars. *Geology*, *10*(3), 147–152. https://doi.org/10.1130/0091-7613(1983)11<55b:carods>2.0.co;2

Howard, A. D. (1994). A detachment-limited model of drainage basin evolution. *Water Resources Research*, *30*(7), 2261–2285. https://doi.org/10.1029/94WR00757

Howard, A. D., Kochel, R. C., & Holt, H. E. (Eds.). (1988). "Groundwater Sapping Experiments and Modeling." In Groundwater Sapping Experiments and Modeling. *Sapping features of the Colorado Plateau: A comparative planetary geology field guide*. 71–83.

Howard, A. D., & Mclane, C. F. (1988). Erosion of cohensionless sediment by groundwater seepage. *Water Resources*, *24*(10), 1659–1674. https://doi.org/10.1029/WR024i010p01659

Kochel, R. C., Howard, A. D., & Mclane, C. F. (1985). Channel networks developed by groundwater sapping in fine-grained sediments: Analogs to some Martian valleys. In M. J. Woldenberg (Ed.), *Models in Geomorphology* (pp. 313–341). Winchester, MA: Allen and Unwin.

Kochel, R. C., & Piper, J. F. (1986). Morphology of large valleys on Hawaii: Evidence for groundwater sapping and comparisons with Martian valleys. *Journal of Geophysical Research*, *91*(B13), E175. https://doi.org/10.1029/jb091ib13p0e175

Kohl, C. P., & Nishiizumi, K. (1992). Chemical isolation of quartz for measurement of in-situ produced cosmogenic nuclides. *Geochimica et Cosmochimica Acta*, *56*(9), 3583–3587.

Kurtz, A. C., Lugolobi, F., & Salvucci, G. (2011). Germanium-silicon as a flow path tracer: Application to the Rio Icacos watershed. *Water Resources Research*, *47*, W06516. https://doi.org/10.1029/2010WR009853

Lague, D. (2014). The stream power river incision model: Evidence, theory and beyond. *Earth Surface Processes and Landforms*, *39*(1), 38–61. https://doi.org/10.1002/esp.3462

Laity, J., & Malin, M. (1985). Sapping processes and the development of theater-headed valley networks on the Colorado Plateau. *Geological Society of America Bulletin*, *96*, 203–217.

Lal, D. (1991). Cosmic ray labeling of erosion surfaces: In situ nuclide production rates and erosion models. *Earth and Planetary Science Letters*, *104*, 424–439.

Lamb, M. P., Howard, A. D., Dietrich, W. E., & Perron, J. T. (2007). Formation of amphitheater-headed valleys by waterfall erosion after large-scale slumping on Hawai'i. *Bulletin of the Geological Society of America*, *119*(7–8), 805–822. https://doi.org/10.1130/B25986.1

Lamb, M. P., Howard, A. D., Johnson, J., Whipple, K. X., Dietrich, W. E., & Perron, J. T. (2006). Can springs cut canyons into rock? *Journal of Geophysical Research*, *111*, E07002. https://doi.org/10.1029/2005JE002663

Larsen, M. C., Torres-Sánchez, A. J., & Concepción, I. M. (1999). Slopewash, surface runoff and fine-litter transport in forest and landslide scars in humid-tropical steeplands, Luquillo Experimental Forest, Puerto Rico. *Earth Surface Processes and Landforms*, *24*(6), 481–502. https://doi.org/10.1002/(SICI)1096-9837(199906)24:6<481::AID-ESP967>3.0.CO;2-G

Luquillo CZO Rio Blanco and Rio Mameyes LiDAR Survey. (2010). https://doi.org/10.5069/G9BZ63ZR

Malin, M. C., & Carr, M. H. (1999). Groundwater formation of martian valleys. *Nature*, *397*(6720), 589–591. https://doi.org/10.1038/17551

Moore, R. D. (2004a). Introduction to salt dilution gauging for streamflow measurement Part 1. *Streamline Watershed Management Bulletin*, *7*(4), 20–23. https://doi.org/10.1592/phco.23.9.1S.32890

Moore, R. D. (2004b). Introduction to salt dilution gauging for streamflow measurement part 2: Constant-rate injection. *Streamline Watershed Management Bulletin*, *8*(1), 1–15. https://doi.org/10.1002/bip.360310619

Murphy, S. F., & Stallard, R. F. (2012). Hydrology and climate for four watersheds in eastern Puerto Rico. In S. F. Murphy & R. F. Stallard (Eds.), *Water quality and landscape processes of four watersheds in eastern Puerto Rico* (pp. 43–84). Reston, VA: US Geological Survey.

Murphy, S. F., Stallard, R. F., Scholl, M. A., González, G., & Torres-Sánchez, A. J. (2017). Reassessing rainfall in the Luquillo Mountains, Puerto Rico: Local and global ecohydrological implications. *PLoS ONE*, *12*(7), 1–26. https://doi.org/10.1371/journal.pone.0180987

Nishiizumi, K., Imamura, M., Caffee, M. W., Southon, J. R., Finkel, R. C., & McAninch, J. (2007). Absolute calibration of 10 Be AMS standards. *Nuclear Instruments and Methods in Physics Research, Section B: Beam Interactions with Materials and Atoms*, *258*(2), 403–413. https://doi.org/10.1016/j.nimb.2007.01.297

Petroff, A. P., Devauchelle, O., Abrams, D. M., Lobkovsky, A. E., Kudrolli, A., & Rothman, D. H. (2011). Geometry of valley growth. *Journal of Fluid Mechanics*, *673*, 245–254. https://doi.org/10.1017/S002211201100053X

Phillips, C. B., & Jerolmack, D. J. (2016). Self-organized river channels are a critical filter on climate signals. *Science*, *352*(6286), 694–697. https://doi.org/10.1126/science.aad3348

Pike, A.S., Scatena, F.N., Wohl, E. (2010). Lithological and fluvial controls on the geomorphology of tropical montane stream channels in Puerto Rico. *Earth Surface Processes and Landforms*, *35*, 1402–1417. https://doi.org/10.1002/esp.1978

Porder, S., Xing, H.X., Brocard, G.Y., Pett-Ridge, J.C., Johnson, A.H., Goldsmith, S. (2015). Linking geomorphology, weathering and cation availability in the Luquillo Mountains of Puerto Rico. *Geoderma*, *249-250*, 100–110. https://doi.org/10.1016/j.geoderma.2015.03.002

Scatena, F. N., & Larsen, M. C. (1991). Physical aspects of hurricane Hugo in Puerto Rico. *Biotropica*, *23*(4), 317–323.

Schaller, M. F., von Blanckenburg, F., Hovius, N., & Kubik, P. W. (2001). Large-scale erosion rates from in situ-produced cosmogenicnuclides in European river sediments. *Earth and Planetary Science Letters*, *188*, 441–458. https://doi.org/10.1039/c5tb01800e

Schellekens, J., Bruijnzeel, L. A., Scatena, F. N., Bink, N. J., & Holwerda, F. (2000). Evaporation from a tropical rain forest, Luquillo Experimental Forest, eastern Puerto Rico. *Water Resources Research*, *36*(8), 2183–2196. https://doi.org/10.1029/2000WR900074

Schellekens, J., Scatena, F. N., Bruijnzeel, L. A., van Dijk, A. I. J. M., Groen, M. M. A., & van Hogezand, R. J. P. (2004). Stormflow generation in a small rainforest catchment in the Luquillo experimental forest, Puerto Rico. *Hydrological Processes*, *18*, 505–530. https://doi.org/10.1002/hyp.1335

Scholl, M. A., Shanley, J. B., Murphy, S. F., Willenbring, J. K., Occhi, M., & González, G. (2015). Stable-isotope and solute-chemistry approaches to flow characterization in a forested tropical watershed, Luquillo Mountains, Puerto Rico. *Applied Geochemistry*, *63*, 484–497. https://doi.org/10.1016/j.apgeochem.2015.03.008

Schwanghart, W., & Scherler, D. (2014). Short communication: TopoToolbox 2—MATLAB-based software for topographic analysis and modeling in Earth surface sciences. *Earth Surface Dynamics*, *2*(1), 1–7. https://doi.org/10.5194/esurf-2-1-2014

Shanley, J. B., McDowell, W. H., & Stallard, R. F. (2011). Long-term patterns and short-term dynamics of stream solutes and suspended sediment in a rapidly weathering tropical watershed. *Water Resources Research*, *47*. https://doi.org/10.1029/2010WR009788

Sharp, R. P., & Malin, M. C. (1975). Channels on Mars. *Bulletin of the Geological Society of America*, *86*(5), 593–609. https://doi.org/10.1130/0016-7606(1975)86<593:COM>2.0.CO;2

Simon, A., Larsen, M. C., & Hupp, C. R. (1990). The role of soil processes in determining mechanisms of slope failure and hillslope development in a humid-tropical forest eastern Puerto Rico. *Geomorphology*, *3*, 263–286. https://doi.org/10.1016/0169-555X(90)90007-D

Sklar, L. S., & Dietrich, W. E. (1998). River longitudinal profiles and bedrock incision models: Stream power and the influence of sediment supply. *Geophysical Monograph-American Geophysical Union*, *107*, 237–260.

Stallard, R. F. (2012a). Atmospheric inputs to watersheds of the Luquillo Mountains in Eastern Puerto Rico. In S. F. Murphy & R. F. Stallard (Eds.), *Water Quality and Landscape Processes in Four Watersheds in Eastern Puerto Rico* (Vol. 1789-D, pp. 89–112). Reston, VA: US Geological Survey.

Stallard, R. F. (2012b). Weathering, landscape equilibrium, and carbon in four watersheds in eastern Puerto Rico Puerto Rico. In S. F. Murphy & R. F. Stallard (Eds.), *Water Quality and Landscape Processes of Four Watersheds in Eastern Puerto Rico* (pp. 199–248). Reston, VA: US Geological Survey.

von Blanckenburg, F. (2004). Cosmogenic nuclide evidence for low weathering and denudation in the wet, tropical highlands of Sri Lanka. *Journal of Geophysical Research*, *109*, F03008. https://doi.org/10.1029/2003jf000049

Weissel, J. K., & Seidl, M. A. (1997). Influence of rock strength properties on escarpment retreat across passive continental margins. *Geology*, *25*(7), 631–634. https://doi.org/10.1130/0091-7613(1997)025<0631:IORSPO>2.3.CO;2

Whipple, K. X., & Tucker, G. E. (1999). Dynamics of the stream-power river incision model: Implications for height limits of mountain ranges, landscape response timescales, and research needs. *Journal of Geophysical Research*, *104*(B8), 17,661–17,674. https://doi.org/10.1029/1999JB900120

White, A. F., Blum, A., Schulz, M. S., Vivit, D. V., Stonestrom, D. A., Larsen, M. C., et al. (1998). Chemical weathering in a tropical watershed, Luquillo Mountains, Puerto Rico: I. Long-term versus short-term weathering fluxes. *Geochimica et Cosmochimica Acta*, *62*(2), 209–226.